Brodogradnja Volume 76 Number 1 (2025) 76105

journal homepage: www.brodogradnja.fsb.hr

Brodogradnja

An International Journal of Naval Architecture and Ocean Engineering for Research and Development

Uncertainty quantification and global sensitivity analysis of turbulence model closure coefficients for sheet cavity flow around a hydrofoil

Simone Romani, Mitja Morgut *, *Lucia Parussini, Marzio Piller*

Department of Engineering and Architecture, University of Trieste, 34127 Trieste, Italy

ARTICLE INFO

Keywords:
Uncertainty quantification
Polynomial Chaos Expansion
Turbulence model
Cavitation
Hydrofoil

ABSTRACT

This paper presents the uncertainty quantification and sensitivity analysis of the standard k-ε turbulence model applied to the numerical prediction of the non-cavitating and cavitating flow around a 2D NACA66MOD hydrofoil. The turbulence model parameters are treated as epistemic uncertain variables, and the forward propagation of uncertainty is evaluated using the non-intrusive polynomial chaos approach. The required simulations are performed using a commercial CFD solver. The Sobol indices are used to rank the relative contribution of closure coefficients to the total uncertainty in the output quantities. For the considered case, the ranking of the model parameters is not influenced by the presence of the sheet cavity flow, while it varies with respect to the considered output quantity.

1. Introduction

Cavitation is the phenomenon that consists in the formation and activity of cavities (or bubbles) inside a liquid medium [1]. In flowing liquids, cavitation occurs in low-pressure regions where pressure, influenced by the system's geometry, drops below a certain threshold value. Cavitation usually induces negative design effects such as hydrodynamic losses, efficiency reduction, noise, erosion and vibration.

In the case of the hydrofoil, in general, cavitation appears on the hydrofoil suction side and, depending on the flow condition, different types of cavitation may develop [2]. An attached sheet cavity flow develops on the suction side of the NACA66MOD hydrofoil under the flow conditions considered in this study [3].

In addition to the experimental studies, different numerical approaches have been employed to predict and study the cavitation phenomena, including those around hydrofoils as well as relevant marine engineering applications such as marine propellers [4, 5].

Moreover, recently, uncertainty quantification in CFD (Computational Fluid Dynamics) has been growing in interest. Several studies have been carried out in order to quantify the possible impact of both parametric and physical uncertainties on numerical predictions. Among others, in the specific case of bidimensional cavitating flow simulations, Congedo et al. [6] presented an uncertainty assessment on inlet

* Corresponding author.
E-mail address: mmorgut@units.it

http://dx.doi.org/10.21278/brod76105
Received 25.07.2024; Received in revised form 12.11.2024; Accepted 29.11.2024;
Available online 09.12.2024
ISSN 0007-215X; eISSN 1845-5859

and turbulence and cavitation model parameters considering sheet cavitation in a venturi geometry. For the same case, Bae et al. [7] studied the uncertainty propagation related to inlet velocity and wall roughness. Kara et al. [8] estimated the combined effect of uncertainties related to angle of attack, cavitation number and spatial discretization (grid) on a NACA66 hydrofoil [9].

In this study, we have estimated the effect of the uncertainties related to turbulence model parameters on the NACA66MOD hydrofoil [3]. We have employed the RANS (Reynolds Averaged Navier Stokes) approach combined with a VOF (Volume of Fluid) method, and evaluated the possible impact of uncertainties, related to the standard k-ε turbulence model parameters on two selected output values, i.e. lift coefficient, C_l, and drag coefficient, C_d. To model the mass transfer rate due to cavitation, the Schnerr-Sauer model [10, 11] has been used.

Different techniques can be used to quantify uncertainty [12-14]. For the specific case of model uncertainties in RANS simulations, a very comprehensive review can be found in [15]. Here, to evaluate the forward propagation of the uncertainties related to the parameters (constants) of the standard k-ε turbulence model, we have applied the Sobol Decomposition to the Polynomial Chaos Expansion (here, for brevity, PCE) representation of the distribution of the output values. Polynomial Chaos Expansion is a Response Surface Method (RSM), which is a statistical method to solve multivariate problems by using reasonable experimental design methods and obtaining certain data through experiments [16]. The Polynomial Chaos representation can be derived by intrusive or non-intrusive approaches; only the latter preserves the original governing equations of the model. In this study, the Non-Intrusive PCE approach has been used [17]. The uncertainties have been treated as epistemic, and the samples (collocation points) have been established using the Latin Hypercube Sampling (LHS) strategy [18]. The Sobol indices have been used to rank the relative contribution of closure coefficients in the RANS model to the total uncertainty in lift, C_l, and drag, C_d coefficients.

The above UQ-methodology has been driven by UQLab – The Framework for Uncertainty Quantification [19], and the required simulations have been performed using Simcenter STAR CCM+, a commercial CFD solver [20].

In this study, PCE has been applied progressively increasing the polynomial order from two to five. The effect of the polynomial order on the construction of the PCE response surface has been monitored through the evaluation of the Leave-One-Out Cross-Validation error [21].

The Sobol indices, used to rank the contributions of turbulence model parameters, were very similar in the case of the second and fifth polynomial order. As a matter of fact, here, the ranking of model parameters (the distribution of Sobol indices) has been independent of the polynomial order. The ranking of Sobol indices is unaffected by the flow regime, whether wetted or cavitating, while it differs for C_d and C_l; for the considered case, the uncertainties propagate similarly for fully-wetted flow and steady sheet cavity flow.

The paper is organized as follows. The mathematical model used in CFD simulations is first described; the turbulence model parameters involved and the related uncertainty ranges are provided. Then, the mathematical basis of the PCE is presented. Next, the strategy adopted to practically perform the study is discussed, followed by the presentation of the obtained results. Finally, the concluding remarks are formulated.

2. Mathematical model for CFD simulations.

2.1 Governing equations

The numerical simulations, as previously mentioned, have been carried out employing the RANS (Reynolds Averaged Navier Stokes) turbulence model combined with the VOF (Volume of Fluid) method, according to the following set of governing equations:

$$\nabla \cdot \boldsymbol{V} = \dot{m}\left(\frac{1}{\rho_l} - \frac{1}{\rho_v}\right) \tag{1}$$

$$\frac{\partial(\rho \boldsymbol{V})}{\partial t} + \nabla \cdot (\rho \boldsymbol{V}\boldsymbol{V}) = -\nabla P - \nabla \cdot \{(\mu + \mu_\tau)\,[\,\nabla \boldsymbol{V} + (\nabla \boldsymbol{V})^T]\,\} \tag{2}$$

$$\frac{\partial \alpha}{\partial t} + \nabla \cdot (\alpha \boldsymbol{V}) = \frac{\dot{m}}{\rho_v} \tag{3}$$

In the above equations the phases are considered incompressible (i.e. water, ρ_l, and water vapour density, ρ_v, are constant) and share the same time averaged mixture velocity field $\boldsymbol{V}$**.** Moreover, P is the time averaged pressure, $\dot{m}$ is the interphase mass transfer rate due to cavitation, μ_τ is the turbulent viscosity (evaluated using the turbulence model), α is water vapour volume fraction defined on each computational cell as:

$$\alpha = \frac{Volume\ Water\ Vapour}{Total\ cell\ volume} \tag{4}$$

and it is used to determine the mixture dynamic viscosity, μ, and density, ρ, as:

$$\rho = \alpha \rho_v + (1 - \alpha)\rho_l \tag{5}$$

$$\mu = \alpha \mu_v + (1 - \alpha)\mu_l \tag{6}$$

2.2 Turbulence model

The standard k-ε turbulence model has been used to derive the turbulent viscosity, μ_τ, as a function of turbulence kinetic energy, k, and turbulence dissipation rate, ε. The distribution of k and ε throughout the flow field is governed by the following transport equations [22]:

$$\frac{\partial}{\partial t}(\rho k) + \nabla \cdot (\rho \boldsymbol{V} k) = \nabla \cdot \left[\left(\mu + \frac{\mu_t}{\sigma_k}\right)\nabla k\right] + P_k - \rho\varepsilon \tag{7}$$

$$\frac{\partial}{\partial t}(\rho \varepsilon) + \nabla \cdot (\rho \boldsymbol{V} \varepsilon) = \nabla \cdot \left[\left(\mu + \frac{\mu_t}{\sigma_\varepsilon}\right)\nabla \varepsilon\right] + C_{\varepsilon_1}\frac{\varepsilon}{k}P_k - C_{\varepsilon_2}\rho\frac{\varepsilon^2}{k} \tag{8}$$

The turbulent viscosity is related to k and ε as:

$$\mu_t = \rho C_\mu \frac{k^2}{\varepsilon} \tag{9}$$

The uncertainty related to the model constants $\left(C_\mu, C_{\varepsilon_1}, C_{\varepsilon_2}, \sigma_k, \sigma_\varepsilon\right)$ has been investigated within the ranges provided in Table 1, representing also *standard* values assumed for the aforementioned model constants [23].

Table 1. Intervals of k-ε coefficients

Coefficient	*Lower Bound*	*Upper Bound*	*Interval*	*Standard*
C_μ	0.050	0.150	0.100	0.090
σ_k	0.800	1.400	0.600	1.000
C_{ε_1}	1.000	1.500	0.500	1.440
C_{ε_2}	1.500	3.000	1.500	1.920
σ_ε	0.290	1.500	1.210	1.300

We clarify that the ranges for C_μ, C_{ε_1}, C_{ε_2}, σ_k have been set according to [24], while for the determination of the sensitivity interval of σ_ε, the lower and upper bounds of C_μ, C_{ε_1}, C_{ε_2} have been alternatively used in the following equation [25]

$$\sigma_\varepsilon = \frac{\kappa^2}{C_\mu^{\frac{1}{2}}\left(C_{\varepsilon_2} - C_{\varepsilon_1}\right)} \tag{10}$$

with $\kappa = 0.41$ being the Von Karman constant.

2.3 Interphase mass transfer rate

As for the computation of the interphase mass transfer rate due to cavitation, $\dot{m}$, in this study, a native model available in Simcenter STAR-CCM+, i.e. the Scherr and Sauer model [26, 27], has been employed.

3. Uncertainty quantification and sensitivity analysis

In the following, the PCE method is described along with the Sobol indices used to rank the parameters. The Leave-One-Out Cross-Validation error used to evaluate the accuracy of the PCE response surface is also presented.

3.1 Polynomial Chaos Expansion

The Polynomial Chaos Expansion is a *Stochastic finite element method* based on the spectral representation of uncertainty. In particular, given a vector of deterministic variables $\boldsymbol{x} = (x_1, \dots, x_m)$ and a vector of random variables $\boldsymbol{\xi} = (\xi_1, \dots, \xi_n)$, the general stochastic response function $Y(\boldsymbol{x}, \boldsymbol{\xi})$ can be expressed with a truncated polynomial series where the discrete sum is evaluated over (M+1) output modes [6, 13, 28, 29]:

$$Y(\boldsymbol{x}, \boldsymbol{\xi}) \approx \sum_{i=0}^{M} \alpha_i(\boldsymbol{x}) \varphi_i(\boldsymbol{\xi}) \tag{11}$$

where $\alpha_i(\boldsymbol{x})$ are the deterministic Polynomial Chaos coefficient, and $\varphi_i(\boldsymbol{\xi})$ are multivariate orthogonal polynomials. In the specific case of uniformly distributed input variables defined over a hyperrectangular domain, the Legendre polynomials are used.

3.1.1 Point-Collocation Non-Intrusive Polynomial Chaos approach

Using a non-intrusive approach, the unknown PCE coefficients, $\alpha_i(\boldsymbol{x})$, can be determined as follows. First, the number of the required collocation points (samples), K, have to be evaluated. They can be determined as:

$$K = n_p \frac{(n+p)!}{n!\, p!} = n_p(M+1) \tag{12}$$

where n is the number of random input variables, p, is the degree of the polynomial chaos, and $n_p = 2$ is the oversampling ratio [30-32].

Then, for each collocation point (here, a certain combination of values of turbulence model parameters), responses (here, C_d and C_l) are evaluated by the direct resolution of the governing equations (here, performing a CFD simulation). Eventually, the resulting linear system (13) [33, 34] is solved in least-squares sense to obtain the $\alpha_i(\boldsymbol{x})$ coefficients. In the context of this study, the LARS algorithm [35] has been used.

$$\begin{Bmatrix} Y(\boldsymbol{x}, \boldsymbol{\xi}_0) \\ \vdots \\ Y(\boldsymbol{x}, \boldsymbol{\xi}_{K-1}) \end{Bmatrix} = \begin{bmatrix} \varphi_0(\boldsymbol{\xi}_0) & \cdots & \varphi_M(\boldsymbol{\xi}_0) \\ \vdots & \ddots & \vdots \\ \varphi_0(\boldsymbol{\xi}_{K-1}) & \cdots & \varphi_M(\boldsymbol{\xi}_{K-1}) \end{bmatrix} \begin{Bmatrix} \alpha_0(\boldsymbol{x}) \\ \vdots \\ \alpha_M(\boldsymbol{x}) \end{Bmatrix} \tag{13}$$

3.1.2 Statistics and Sobol indices

In the case of the Legendre PCE, the mean value μ_{PC}, partial variances $D_{i_1,\dots,i_s}$ and the total variance D of responses can be evaluated as [29, 34, 36]:

$$\mu_{PC} = \int_{\Omega} Y(\boldsymbol{x}, \boldsymbol{\xi})\, d\boldsymbol{\xi} = \alpha_0(\boldsymbol{x}) \tag{14}$$

$$D = \sigma_{std}^2 = \int_{\Omega} [Y(\boldsymbol{x}, \boldsymbol{\xi}) - \mu_{PC}]^2\, d\boldsymbol{\xi} = \sum_{i=1}^{M} \alpha_i^2(\boldsymbol{x}) \tag{15}$$

$$D_{i_1,\dots,i_s} = \sum_{\boldsymbol{m} \in \mathcal{I}} \alpha_{\boldsymbol{m}}^2(\boldsymbol{x}) \tag{16}$$

$$\boldsymbol{\mathcal{I}} = \{\boldsymbol{m} \in (1,\dots,M): k \in (i_1,\dots,i_s) \Leftrightarrow m_k \neq 0\} \tag{17}$$

where Ω is the support region of random input variables.

The main effect Sobol indices and interactions are evaluated as [37, 38]:

$$S_{i_1,\dots,i_s} = \frac{D_{i_1,\dots,i_s}}{D} \tag{18}$$

while the total Sobol indices are determined as:

$$S_i^T = \sum_{i \subset (i_1,\dots,i_s)} S_{i_1,\dots,i_s} \tag{19}$$

It should be noted that Sobol indices are simply the ratio between partial variances and the total variance. They can be evaluated for both single random variables, S_i, and interaction between variables, S_{ij} , and the below property is satisfied [39, 40]:

$$\sum_{i=1}^{n} S_i + \sum_{1 \le i < j \le n}^{n-1} S_{ij} + \cdots + S_{1,\dots,n} = 1 \tag{20}$$

The Sobol indices are related to the selected Polynomial Chaos degree, in fact for a Polynomial Chaos of the second order we can compute the Sobol indices of single (main) coefficients and two-way interactions, for a Polynomial Chaos of the third order we can compute the Sobol Indices of single variables, two-way and three-way interactions.

For the sake of completeness, we point out that main Sobol indices above 0.2 typically suggest a significant influence on the output. Variables with high indices are critical to the fluid dynamic model and warrant close attention.

3.2 Leave-One-Out Cross-Validation error.

In order to monitor the performance of PCE, corresponding to a given order, the Leave-One-Out (LOO) Cross-Validation error, ε_{LOO} , has been evaluated [35]:

$$\varepsilon_{LOO} = \frac{\sum_{i=0}^{K-1}\left[\mathcal{M}(\boldsymbol{x},\boldsymbol{\xi}_i) - \mathcal{M}_{PC\setminus i}(\boldsymbol{x},\boldsymbol{\xi}_i)\right]^2}{\sum_{i=0}^{K-1}[\mathcal{M}(\boldsymbol{x},\boldsymbol{\xi}_i) - \mu_{PC}]^2} \tag{21}$$

In the above equation, $\mathcal{M}(\boldsymbol{x},\boldsymbol{\xi}_i)$ is the response value obtained with a CFD simulation for the *i*-th collocation point (certain combination of input parameters) and $\mathcal{M}_{PC\setminus i}(\boldsymbol{x},\boldsymbol{\xi}_i)$ is the reduced response value obtained with the PCE response surface neglecting the *i*-th collocation point.

ε_{LOO} provides an indication of the expected performance of the model on unobserved data, thus a lower value suggests a better model performance in terms of predictive accuracy and generalization. Let us remark that ε_{LOO}, as defined in equation (21), is not an absolute error but is a relative error, showing how much the model is both accurate and robust to slight variations in the data compared to the variance of the observed data.

4. Numerical framework/strategy

Based on the models described in the previous sections, in this study, a computational strategy similar to [33] has been employed. The non-intrusive PCE method has been applied in three subsequent steps described in the following.

4.1 The Logic of the strategy

Step 1: As a first step the number of the collocation points, K, has been set according to [30, 31] using expression (12). Then, K, combinations of input parameters have been generated using Latin Hypercube Sampling (LHS), and in accordance with ranges provided in section 2.2.

Step 2: CFD simulations have been carried out for the K combinations.

Step 3: The results obtained at step 2 (C_l, C_d for each combination) have been used to determine the PCE coefficients involving the LARS algorithm. Finally, the PCE statistics, as well as sensitivity indices, have been evaluated according to equations (14)-(18). Finally, ε_{LOO} has been evaluated.

In Fig.1 a sketch of the strategy is presented.

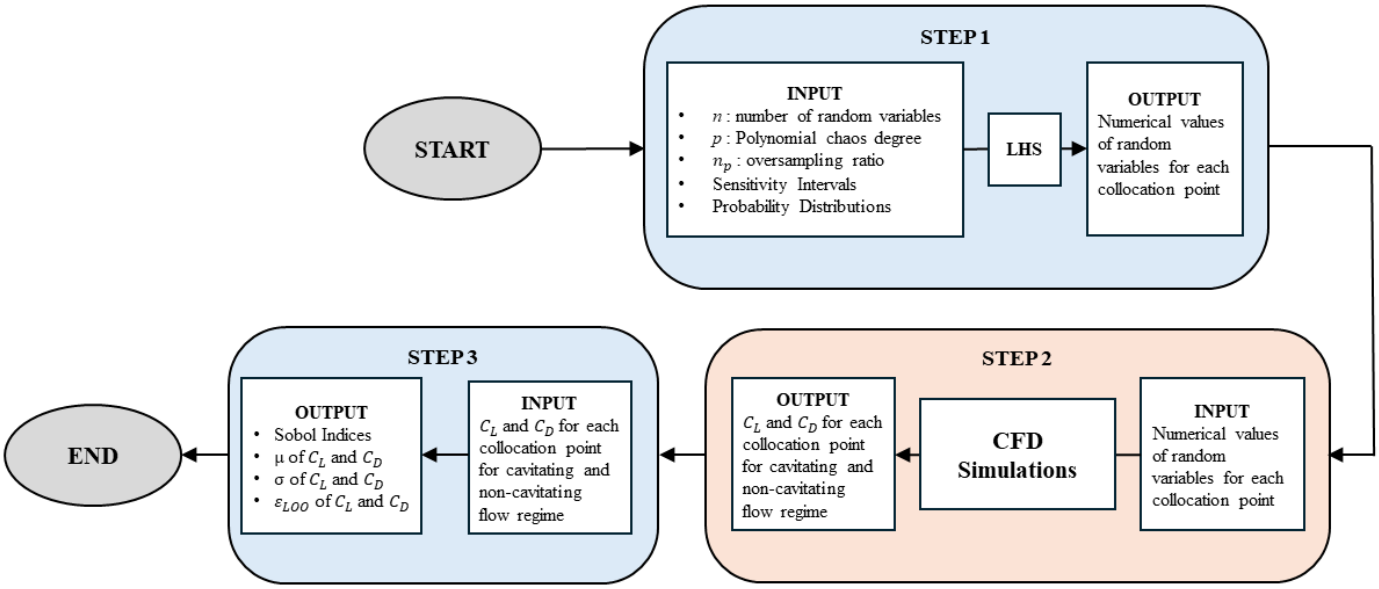

Fig. 1 Logical diagram of the strategy

Here, the overall strategy has been applied 4 times, increasing the order of the PCE from 2 to 5. The number of the required simulations corresponding to different polynomial orders is given by equation (12), where n=5, p ranges from 2 to 5 and n_p=2.

4.2 CFD Setup

To simulate the flow around the hydrofoil, the two-dimensional domain depicted in Fig. 2 has been used.

The computational domain has been spatially discretized using a 2D unstructured polygonal mesher, available in Simcenter STAR-CCM+, with a layer of prismatic cells inflated from the surface of the hydrofoil. The mesh-generation process has been automated and parametrized, so that all the refinement steps, adopted by the current meshing strategy, are linked in relative terms to a given cell base-size. A mesh-sensitivity study has been carried out considering the fully wetted flow condition and using progressively refined meshes, generated using different values of the cell base-size as reported in Table 2. For reasons of computational efficiency, the uncertainty quantification study relies on the coarse mesh. In Fig. 3 a snapshot of the coarse mesh is shown.

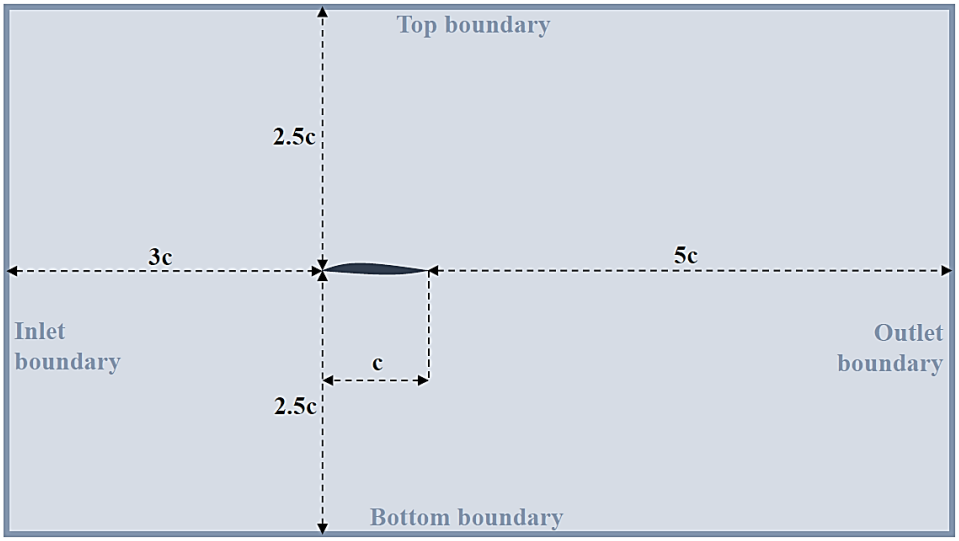

Fig. 2 Sketch of the computational domain

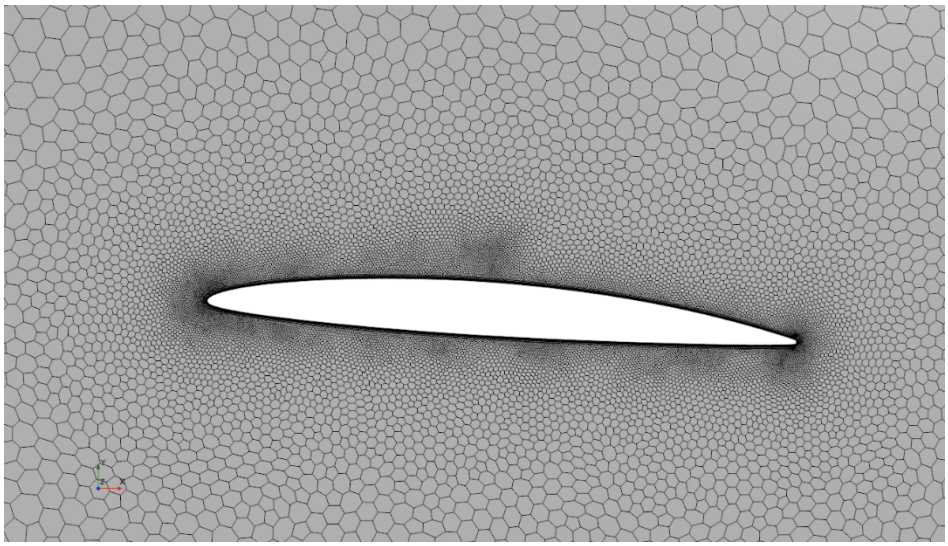

Fig. 3 Mesh close to the hydrofoil

Table 2 Mesh sensitivity study

MESH	Mesh nodes on airfoil	Nr. of cells	Base size for mesh generation [mm]	Min y^+ (max y^+)	C_d	C_l
COARSE (C)	663	32874	10	2.7 (11)	0.0218	0.6151
MEDIUM (M)	1268	81425	5	1.2 (6.2)	0.0242	0.6010
FINE (F)	2477	226455	2.5	0.47 (3.4)	0.0254	0.5949

Moreover, the following boundary conditions have been applied. On the Inlet boundary, according to [41], prescribed values of k and ε, as well as free-stream velocity, V , have been imposed; the value of the vapour volume fraction has been set equal to zero. On the Outlet boundary, a fixed value of static pressure has been imposed. On the solid surfaces of the hydrofoil, as well as on the top and bottom boundaries of the domain, a no-slip boundary condition has been imposed. The simulations have been switched from the fully-wetted flow conditions to the considered cavitating flow regime (i.e. $\sigma = \frac{Pout-Pv}{0.5\,\rho_l\,V^2} = 0.91$) varying the value of the vapour pressure. For water and water-vapour the following characteristics have been set $\rho_l = 997\text{kg/m}^3$, $\mu_l = 8.89324 \times 10^{-4}$ Pa s, $\rho_v = 0.023084$ kg/m^3, $\mu_v = 9.055 \times 10^{-6}$ Pa s. All the simulations have been unsteady, where for the time discretization the second order implicit time scheme has been employed with a time-step equal to 10^{-4} s. It is assumed that steady-state conditions have been attained

once the standard deviation of the drag coefficient over a set of samples spanning the last 3 milliseconds drops below 0.0125% of the average drag coefficient measured over the same time frame.

5. Results

In this section, the results obtained by applying the developed strategy are presented as follows. At first, the convergence rate study, evaluated monitoring ε_{LOO} is presented. Then, the influence of the polynomial order on the mean values, μ_{PC}, of the lift and drag coefficients along with the corresponding standard deviation, σ_{std}, are shown. Finally, the comparison of Sobol Indices, aimed to rank the importance of the single turbulence model constants as well as the importance of interactions between two constants (pairs), on the selected output values C_l, C_d is provided.

5.1 PCE Convergence rate

From the trends shown in Fig. 4, it is possible to notice that, as expected, the value of ε_{LOO} reduces with the increase of the polynomial order. The error reduces monotonically for both considered output values (C_d , C_l). From a general point of view, it is possible to notice that the error is higher for the cavitating flow regime.

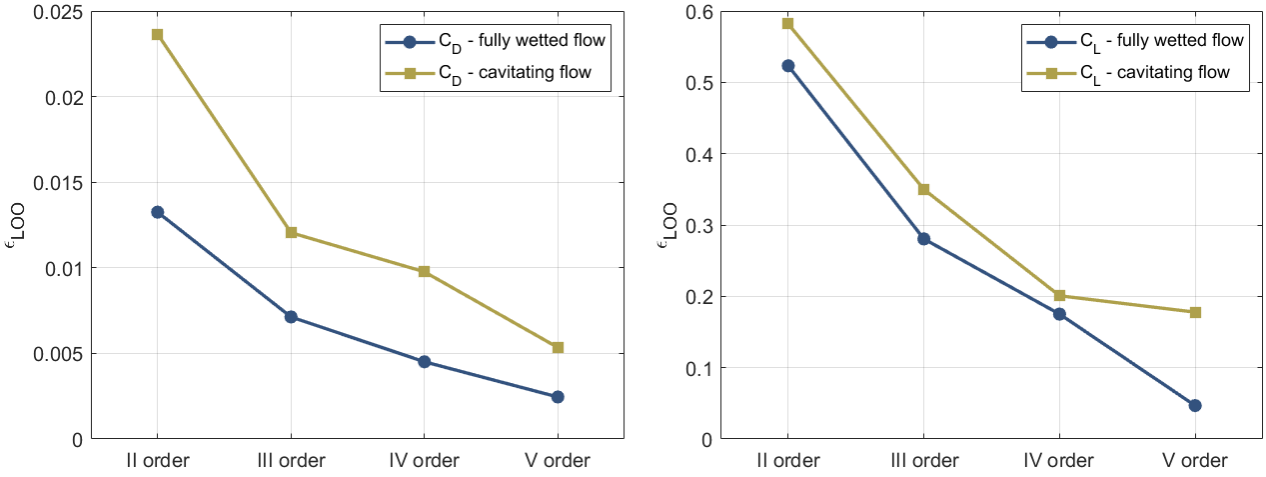

Fig. 4 ε_{LOO} of responses, C_d (left), C_l (right), for the two different flow regimes

5.2 Hydrodynamic characteristics

In Fig. 5, mean values and confidence intervals of responses for the different flow regimes are given. The confidence intervals have been determined by the equation:

$$Confidence\ Interval = \mu_{PC} \pm MOE \tag{22}$$

where the Margin Of Error (MOE) for a 95% confidence interval is given by

$$MOE \equiv 1.96 \frac{\sigma_{std}}{\sqrt{K}} \tag{23}$$

Considering the results for the wetted flow (left column of Fig. 5), a convergent trend can be observed. However, in the case of cavitating flow, the predicted values do not exhibit a convergent trend, principally to the mean C_d and C_l values obtained with the PCE of the fourth order which are overpredicted (considering the expected trend).

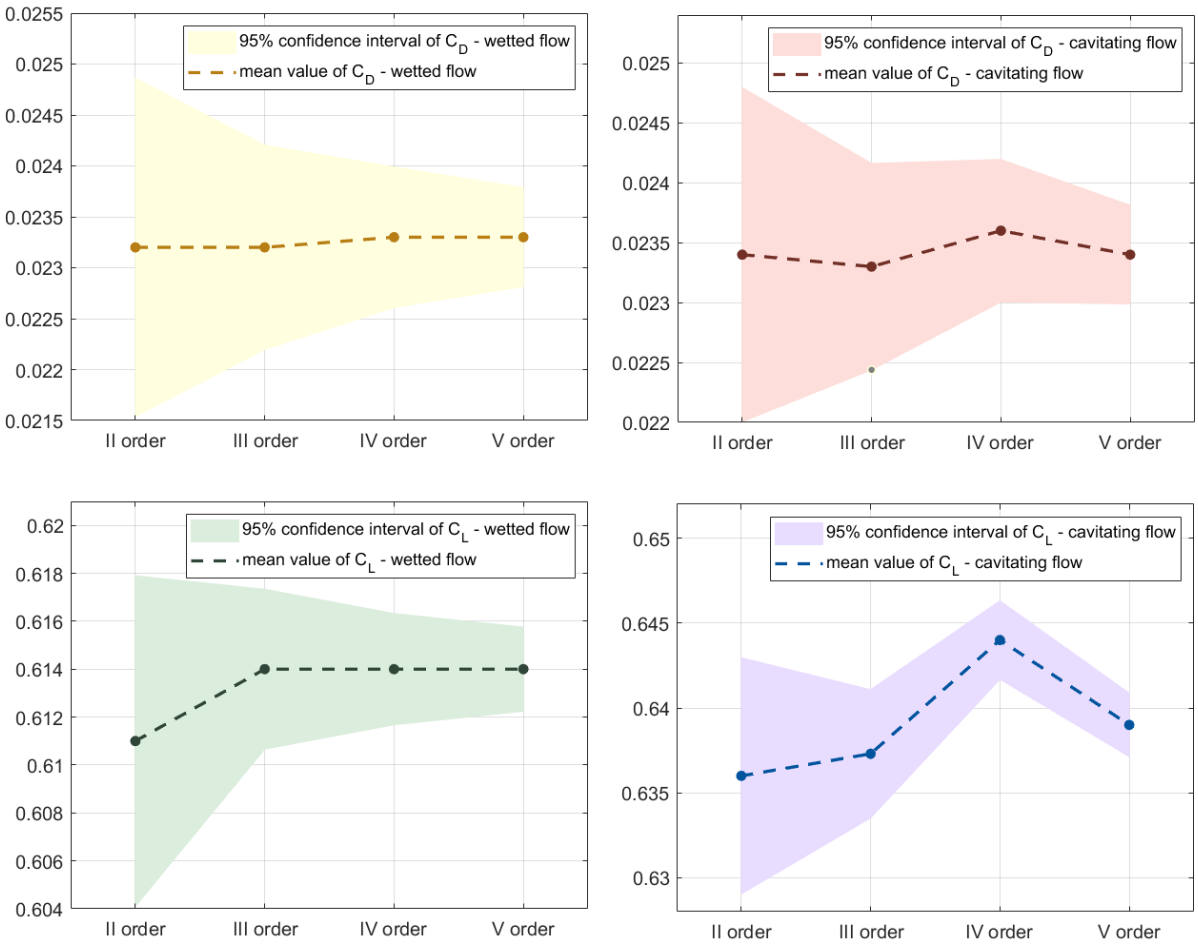

Fig. 5 Mean Values and Confidence Intervals of outputs, C_d,C_l; wetted flow (left), cavitating flow (right)

Finally, it is also possible to note that confidence intervals decrease with the increment of the polynomial order showing the expected trend, i.e., the calculation error of the uncertainty reduces by increasing the polynomial degree.

5.3 Sobol Indices

In the following, the ranking of the single model constants (main parameters) and pairs (two-way interactions), evaluated with reference to C_d, is first presented. Then, a similar analysis is given considering C_l. For the sake of clarity, we point out that in the following figures, the main Sobol indices refer to those evaluated through equation (18), while the total indices refer to those obtained by summing the contributions of the main values and the values of the interactions (see equation (19)). It is important to point out, that for the sake of convenience only the results corresponding to the PCE of the second and fifth order are compared.

5.3.1 Drag coefficient

In Fig. 6 the Sobol indices related to C_d, for fully wetted flow conditions, are shown. It is possible to note that with the PCE of the second and fifth order, the same ranking of indices has been obtained, with the highest values corresponding to σ_ε. It is interesting to point out, that the value of σ_ε is at least double compared to the other coefficients, showing that most of the uncertainty in the calculation of the drag coefficient originates from the model for the turbulent transport of the turbulent dissipation rate.

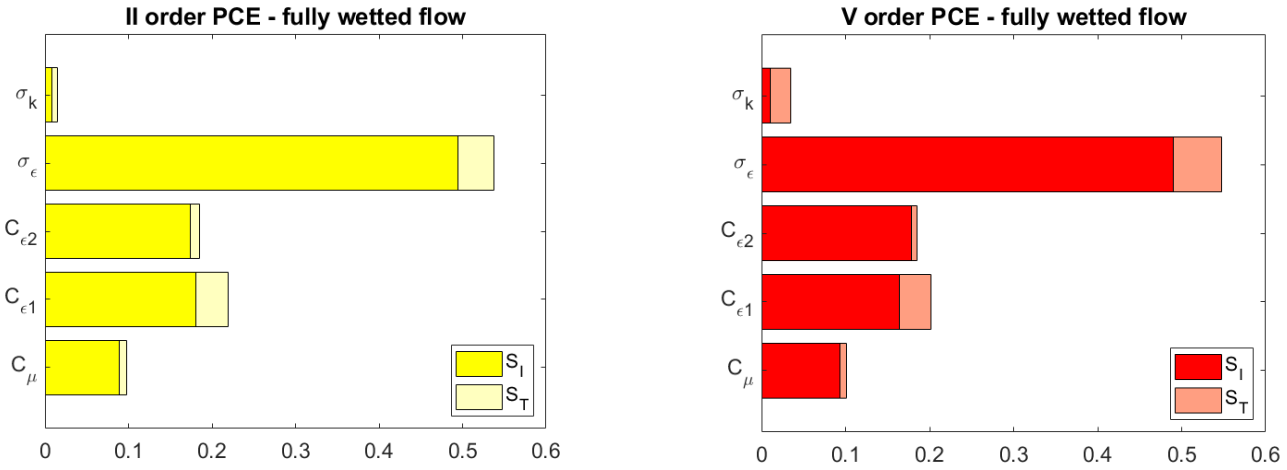

Fig. 6 Main S_I, and total S_T, Sobol Indices of C_d for fully wetted flow; second order PCE (left), fifth order PCE (right)

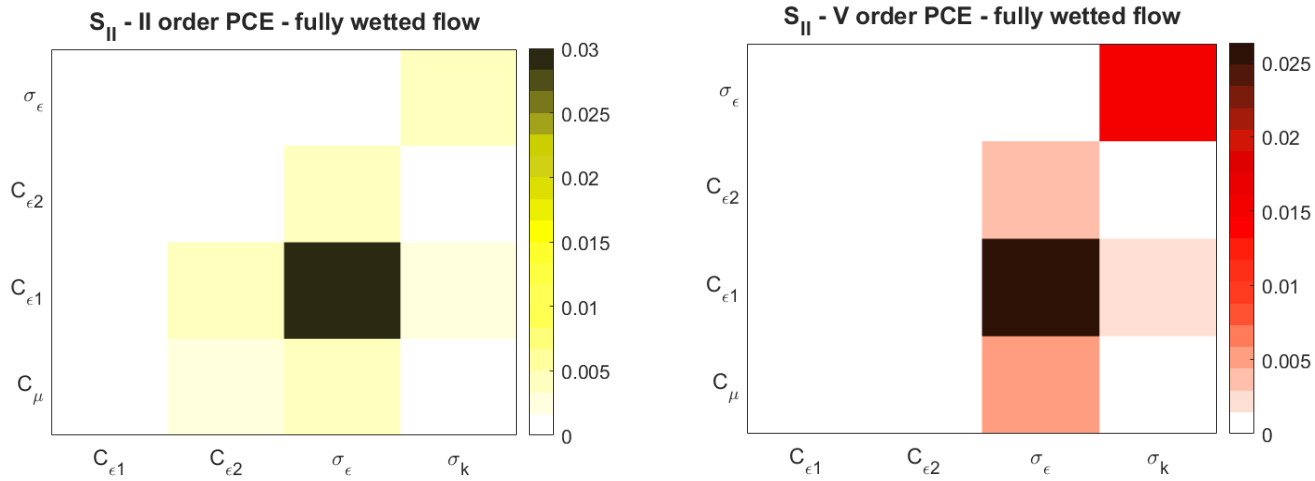

Fig. 7 Ranking of pairs S_{II} (two-way interactions) of C_d for fully wetted flow; second order PCE (left), fifth order PCE (right)

As for the ranking of two-way interactions, from Fig. 7 it is possible to observe that, in this case, the pair which seems to mostly influence the prediction of drag is $C_{\varepsilon_1} - \sigma_\varepsilon$. The ranking of the most intense interactions, i.e. $C_{\varepsilon_1} - \sigma_\varepsilon$ and $\sigma_k - \sigma_\varepsilon$, is consistent between the second- and the fifth-order PCE representations.

Considering the results presented in Fig. 8 and Fig. 9, it is possible to observe that, also for the cavitating flow regime, the parameter with the highest weight is σ_ε and the two-way interaction which seems to influence most the results is still $C_{\varepsilon_1} - \sigma_\varepsilon$. As a matter of fact, it seems that the ranking of the model constants is not influenced by the presence of the attached sheet cavity.

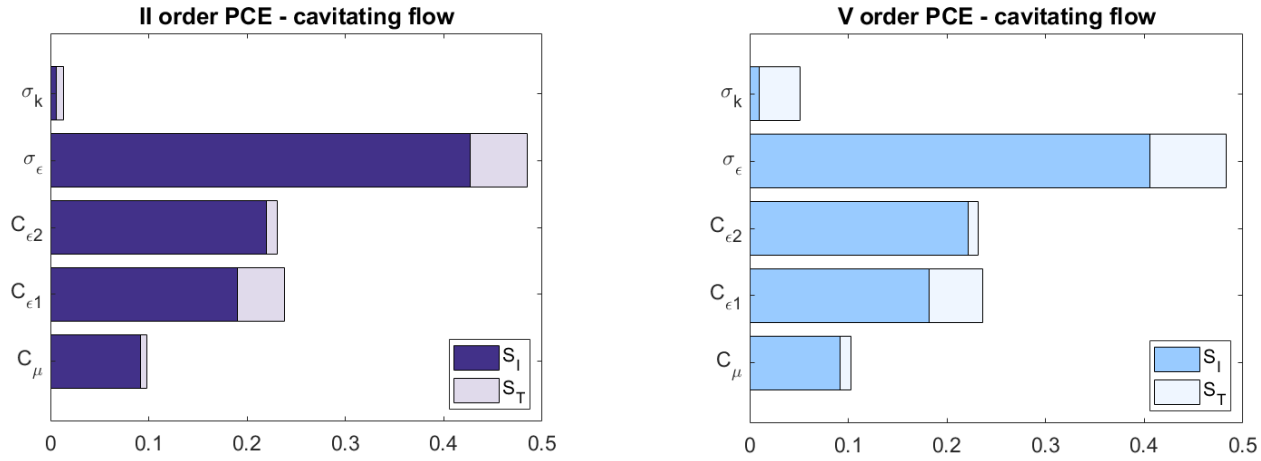

Fig. 8 Main S_I, and total S_T, Sobol Indices of C_d for cavitating flow; second order PCE (left), fifth order PCE (right)

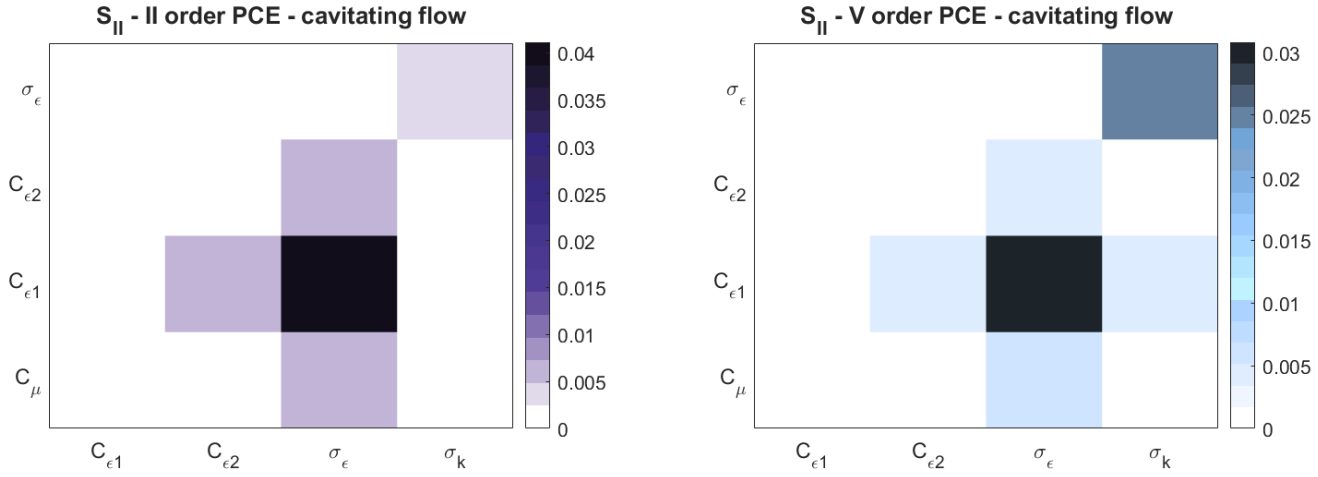

Fig. 9 Ranking of pairs (interactions) of C_d for cavitating flow; second order PCE (left), fifth order PCE (right)

5.3.2 Lift Coefficient

Considering the results related to the lift coefficient, for the fully-wetted flow condition, from Fig. 10 it is possible to note that, in this case, the turbulence model coefficient which seems to have the higher impact on the predictions of lift values is C_{ε_2}. Considering the results related to the pairs (ranking of the importance of the interaction of two parameters) presented in Fig. 11, a dominant interaction is that of pair $C_{\varepsilon_1} - C_{\varepsilon_2}$; other pairs seem to have a very minor/negligible influence. Accordingly, the uncertainty on the lift coefficient is mostly affected by the uncertainty on the modelling of the production (by mean flow) and of the dissipation (by viscous effects) of the turbulent dissipation rate.

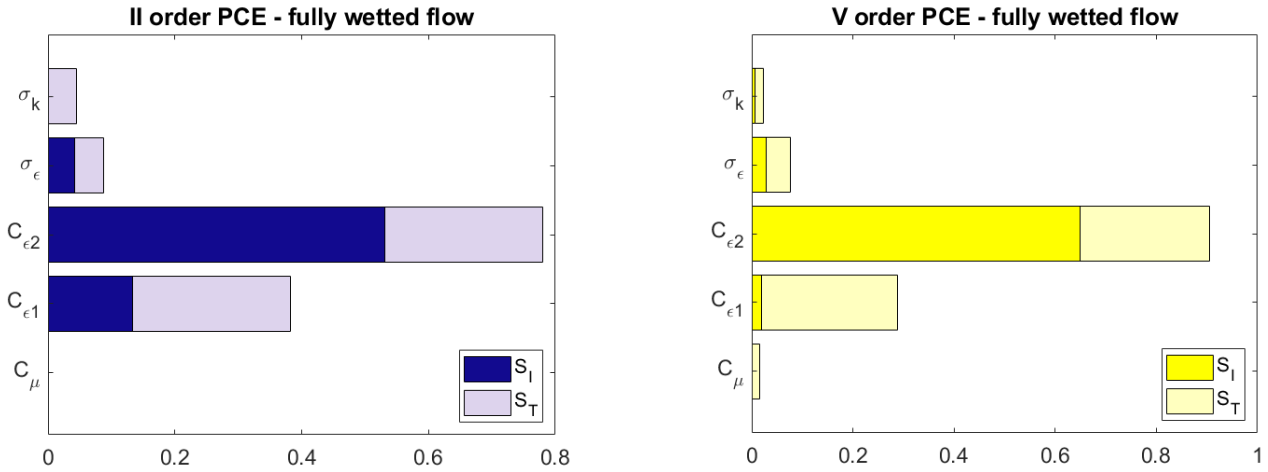

Fig. 10 Main S_I, and total S_T, Sobol Indices of C_l for fully wetted flow; second order PCE (left), fifth order PCE (right)

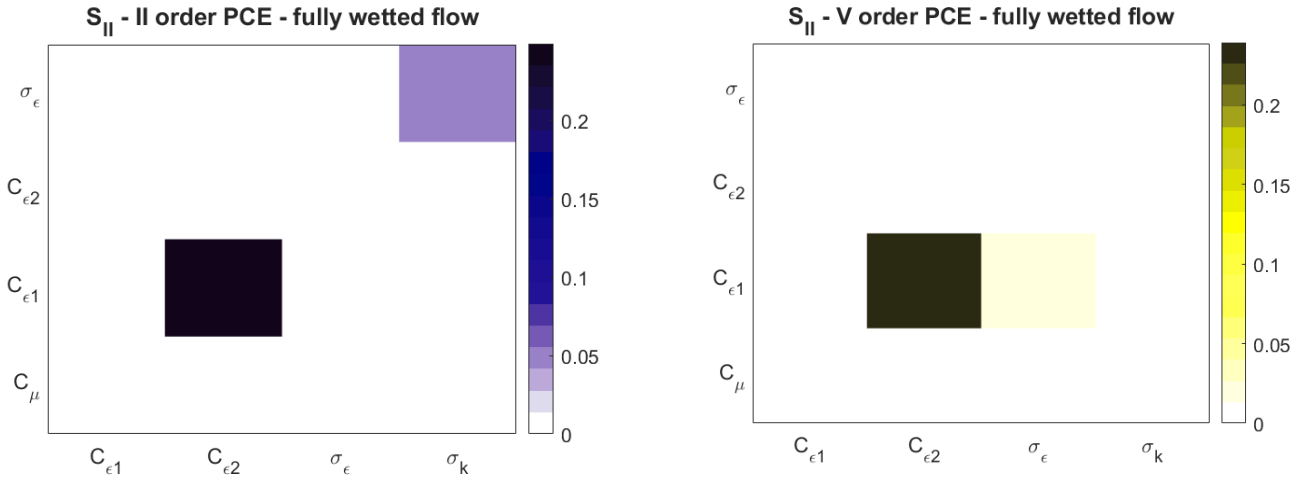

Fig. 11 Ranking of two-way interactions of C_l for fully wetted flow; second order PCE (left), fifth order PCE (right)

As for the cavitating flow regime, Fig. 12 shows a ranking very similar to that obtained for the fully-wetted flow (see Fig. 10), with C_{ε_2} being the parameter with the higher score/ranking. Instead, for two-way interactions, from Fig. 13 it seems that also for the cavitating flow regime the most important interaction is that between parameters $C_{\varepsilon_1} - C_{\varepsilon_2}$.

Generally speaking, it is interesting to note that also in the case of the lift coefficient the ranking has not been influenced by the different flow regimes.

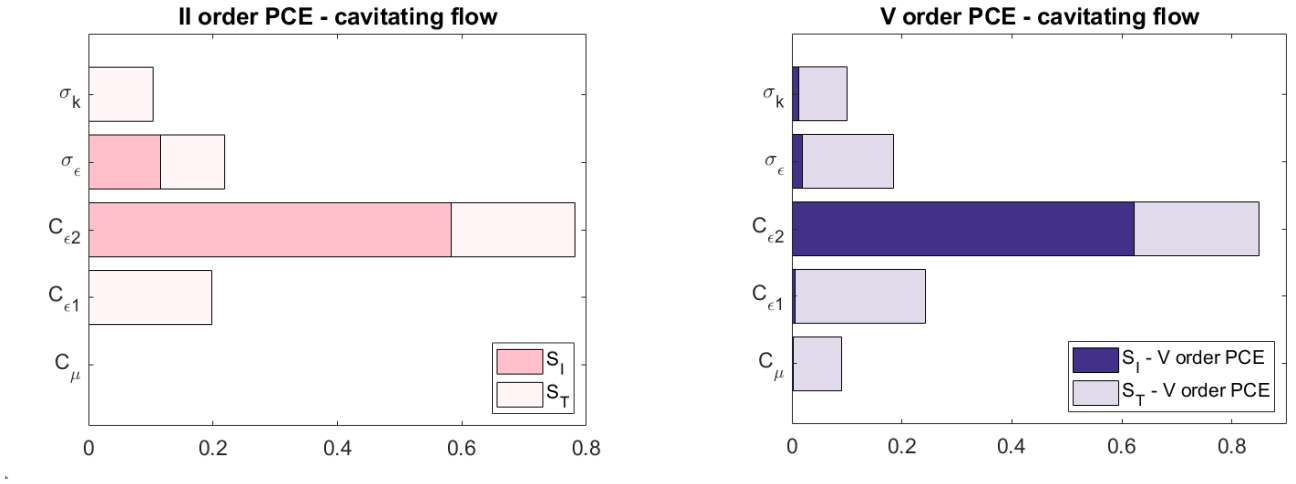

Fig. 12 Main S_I, and total S_T, Sobol Indices of C_l for cavitating flow; second order PCE (left), fifth order PCE (right)

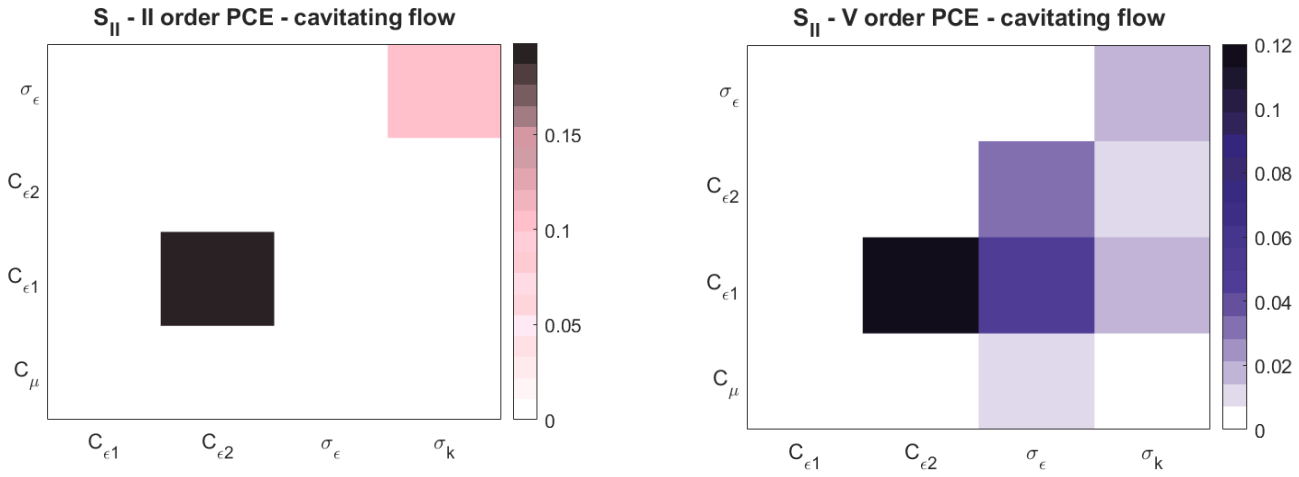

Fig. 13 Ranking of pairs (interactions) of C_l for cavitating flow; second order PCE (left), fifth order PCE (right)

Finally, considering the overall results related to ranking, it seems that, in this case, the flow regime does not influence the weights of variables (the outputs are mainly sensitive to the variation of the same coefficients for both the typologies of flow). In this respect, for the sake of clarity, the most important main parameters and pairs have been collected in Table 3.

Moreover, from the obtained results, the values of the interactions among the parameters of the Standard k-ε turbulence model were higher in the case of the cavitating flow. Thus, for both C_l and C_d the Sobol Indices of total order associated to the cavitating flow are greater than the Sobol Indices of total order associated to the wetted flow.

Table 3 The most important parameters related to Sobol indices (independent of the polynomial order)

	C_d		C_l	
	S_I	S_{II}	S_I	S_{II}
Wetted	σ_ε	$C_{\varepsilon1} - \sigma_\varepsilon$	$C_{\varepsilon2}$	$C_{\varepsilon1} - C_{\varepsilon2}$
Cavitating	σ_ε	$C_{\varepsilon1} - \sigma_\varepsilon$	$C_{\varepsilon2}$	$C_{\varepsilon1} - C_{\varepsilon2}$

6. Conclusions

In this study, the Global Sensitivity Analysis has been applied to the case of the RANS simulations of the flow around the NACA66MOD hydrofoil operating at a given angle of attack (AoA = 4 deg). More precisely, the possible propagation of the uncertainties related to the coefficients of the standard $k-\varepsilon$ turbulence model on the predicted lift and drag coefficients has been evaluated. The study has been conducted for fully wetted flow and a selected cavitating flow regime.

To this aim, we have employed a Polynomial Chaos Expansion based on a Point-Collocation Non-Intrusive approach along with Sobol decomposition. The uncertainties have been treated as epistemic.
The solution strategy, based on PCE and Sobol decomposition, has been implemented using UQLAB (The Framework for the Uncertainty Quantification) and the required simulations have been performed using Simcenter-STAR CCM+.

The study has been repeated varying the polynomial order from two to five and the convergence rate (approximation level) of the generated response surfaces has been monitored by the evaluation of the Leave-One-Out Cross-Validation error.

For the considered case, for the fully-wetted flow conditions, a minor error has been observed compared to the corresponding cavitating flow conditions. For both regimes, the error reduces monotonically with the increase of the polynomial order. However, only minor differences have been observed between the results obtained with the PCE of the second and fifth order, respectively.

Regarding the ranking of the coefficients and pairs some differences have been observed between the results obtained from the analysis performed considering C_d and C_l, respectively. Indeed, in this case, the ranking has not been influenced by the flow regime. As a matter of fact, for the fully-wetted flow condition as well as sheet cavity flow regime, in the case of C_d the dominant main Sobol index is σ_ε while the pair is $C_{\varepsilon_1}-\sigma_\varepsilon$. In the case of C_l the dominant main Sobol index is C_{ε_2}, while for the pair $C_{\varepsilon_1}-C_{\varepsilon_2}$.

REFERENCES

[1] Young, F. R., 1999. Cavitation. *Imperial College Press*, London

[2] Franc, J.-P., Michel, J.-M., 2004. Fundamentals of Cavitation. *Kluwer Academic Publisher*, Dordrecht, Netherlands.

[3] Shen, Y., Dimotakis, P., 1989. The influence of surface cavitation on hydrodynamic forces. *SNAME 22nd American Towing Tank Conference*, 8-11 August, St. John's, Newfoundland, Canada. https://doi.org/10.5957/ATTC-1989-006

[4] SVA. Potsdam Propeller Test Case PPTC. https://www.sva-potsdam.de/en/potsdam-propeller-test-case-pptc/. accessed 7th August 2024.

[5] Bagheri, R. M., Mehdigholi, H., Seif, S. M., Yaakob, O., 2015. An experimental and numerical prediction of marine propeller noise under cavitating and non-cavitating conditions. *Brodogradnja*, 66(2), 29-45.

[6] Congedo, P.M., Goncalves, E., Rodio, M.G., 2015. About the uncertainty quantification of turbulence and cavitation models in cavitating flows simulations. *European Journal of Mechanics B/Fluids*, 53, 190-204. https://doi.org/10.1016/j.euromechflu.2015.05.005

[7] Bae, J.-H., Chang, K., Lee, G.-H., Kim, B.-C., 2022. Bayesian Inference of Cavitation Model Coefficients and Uncertainty Quantification of a Venturi Flow Simulation. *Energies*, 15, 4204. https://doi.org/10.3390/en15124204

[8] Kara, E., Lidtke, A., K., Düz, B., Rijpkema, D., Kinaci, O. K., 2023. Quantifying Uncertainties in Numerical Predictions of Dynamic Cavitation. *UNCECOMP 2023, 5th ECCOMAS Thematic Conference on Uncertainty Quantification in Computational Sciences and Engineering*, 12-14 June, Athens, Greece. https://doi.org/10.7712/120223.10361.19618

[9] Leroux, J-B., Astolfi, J.A., Billard, J.Y., 2004. An Experimental Study of Unsteady Partial Cavitation. *Journal of Fluids Engineering*, 126(1), 94-101. https://doi.org/10.1115/1.1627835

[10] Schnerr, G., Sauer, J., 2001. Physical and Numerical Modeling of Unsteady Cavitation Dynamics. *4th International Conference on Multiphase Flow*, 27 May-1 June, New Orleans, Louisiana, USA.

[11] Perić, M., 2022. Prediction of cavitation on ships. *Brodogradnja*, 73(3), 39-58. https://doi.org/10.21278/brod73303

[12] Xiu, D., 2010. Numerical Methods for Stochastic Computations: A Spectral Method Approach. *Princeton University Press*. https://doi.org/10.1515/9781400835348

[13] Sullivan, T.J., 2015. Introduction to Uncertainty Quantification, *Springer*, Cham, Switzerland. https://doi.org/10.1007/978-3-319-23395-6

[14] Soize, C., 2017. Uncertainty Quantification, *Springer*, Cham, Switzerland. https://doi.org/10.1007/978-3-319-54339-0

[15] Cinnella, P., Xiao, H., 2019. Quantification of model uncertainty in RANS simulations: A review. *Progress in Aerospace Sciences*, 108, 1-31. https://doi.org/10.1016/j.paerosci.2018.10.001

[16] Hou, S., Zhang, Z., Lian, H., Xing, X., Gong, H., Xu, X., 2022. Hull shape optimization of small underwater vehicle based on kriging-based response surface method and multi-objective optimization algorithm. *Brodogradnja*, 73(3), 111-134. https://doi.org/10.21278/brod73307

[17] Schaefer, J., West, T., Hosder, S., Rumsey, C., Carlson, J.-R., Kleb, W., 2015. Uncertainty Quantification of Turbulence Model Closure Coefficients for Transonic Wall-Bounded Flows. *AIAA Computational Fluid Dynamics Conference*, 22-26 June, Dallas, Texas, USA. https://doi.org/10.2514/6.2015-2461

[18] McKay, M.D., Beckman, R.J., Conover, W.J., 1979. Comparison of Three Methods for Selecting Values of Input Variables in the Analysis of Output From a Computer Code. *Technometrics*, 21(2), 239-245. https://doi.org/10.1080/00401706.1979.10489755

[19] UQLab, The Framework for Uncertainty Quantification. https://www.uqlab.com/. accessed 11th November 2024.

[20] Siemens. https://plm.sw.siemens.com/en-US/simcenter/fluids-thermal-simulation/star-ccm/. accessed 11th November 2024.

[21] Marelli, S., Sudret, B., 2014. UQLab: A framework for uncertainty quantification in Matlab. *2nd International Conference on Vulnerability, Risk Analysis and Management (ICVRAM2014)*, 2554-2563, 13-16 July, Liverpool, United Kingdom. https://doi.org/10.1061/9780784413609.257

[22] Moukalled, F., Mangani, L., Darwish, M., 2016. The Finite Volume Method in Computational Fluid Dynamics, *Springer,* Cham, Switzerland. https://doi.org/10.1007/978-3-319-16874-6

[23] Launder, B.E., Spalding, D.B., 1974. The Numerical Computation of Turbulent Flows. *Computer Methods in Applied Mechanics and Engineering*, 3(2), 269-289. https://doi.org/10.1016/0045-7825(74)90029-2

[24] Shirzadi, M., Mirzaei, P.A., Naghashzadegan, M., 2017. Improvement of k-epsilon model for CFD simulation of atmospheric boundary layer around a high-rise building using stochastic optimization and Monte Carlo Sampling technique. *Journal of Wind Engineering and Industrial Aerodynamics*, 171, 366-379. https://doi.org/10.1016/j.jweia.2017.10.005

[25] Pope, S.B., 2000. Turbulent flows. Cambridge University Press. https://doi.org/10.1017/CBO9780511840531

[26] Siemens. Simcenter STAR-CCM+ Documentation Version 2402. *Siemens Digital Industries Software*, 2024.

[27] Gaggero, G., Villa, D., 2017. Steady cavitating propeller performance by using OpenFOAM, StarCCM+ and a boundary element method. *Proceedings of the Institution of Mechanical Engineers Part M: Journal of Engineering for the Maritime Environment*, 231(2), 411-440. https://doi.org/10.1177/1475090216644280

[28] Sudret, B., 2008. Global sensitivity analysis using polynomial chaos expansions. *Reliability Engineering & System Safety*, 93(7), 964-979. https://doi.org/10.1016/j.ress.2007.04.002

[29] Kaintura, A., Dhaene, T., Spina, D., 2018. Review of Polynomial Chaos-Based Methods for Uncertainty Quantification in Modern Integrated circuits. *Electronics*, 7(3), 30. https://doi.org/10.3390/electronics7030030

[30] Zhang, K., Li, J., Zeng, F., Wang, Q., Yan, C., 2022. Uncertainty Analysis of Parameters in SST Turbulence Model for Shock wave-Boundary Layer Interaction. *Aerospace*, 9(2), 55. https://doi.org/10.3390/aerospace9020055

[31] Hosder, S., Walters, R., 2007. Non-Intrusive Polynomial Chaos Methods for Stochastic CFD - Theory and Applications. *Computational Uncertainty in Military Vehicle Design*, 47, Neuilly-sur-Seine, France.

[32] Yang, J.-T., Li, Y., Li, J.-P., Yan, C., 2023. Uncertainty quantification of SSG/LRR-ω turbulence model closure coefficients. *Acta Astronautica*, 211, 177-191. https://doi.org/10.1016/j.actaastro.2023.06.006

[33] Zhao, Y., Yan, C., Liu, H., Zhang, K., 2019. Uncertainty and sensitivity analysis of flow parameters for transition models on hypersonic flows. *International Journal of Heat and Mass Transfer*, 135, 1286-1299. https://doi.org/10.1016/j.ijheatmasstransfer.2019.02.071

[34] Eck, V.G., Donders, W., Sturdy, J., Feinberg, J., Delhaas, T., Hellevik, L.R., Huberts, W., 2016. A guide to uncertainty quantification and sensitivity analysis for cardiovascular applications. *International Journal for Numerical Methods in Biomedical Engineering*, 32(8). https://doi.org/10.1002/cnm.2755

[35] Marelli, S., Lüthen, N., Sudret, B., 2024. UQLab user manual – Polynomial chaos expansions, Report UQLab-V2.1-104, Chair of Risk, Safety and Uncertainty Quantification, *ETH Zurich*, Switzerland.

[36] Xia, L., Zou, Z.-J., Wang, Z.-H., Zou, L., Gao, H., 2021. Surrogate model-based uncertainty quantification of CFD simulations of the viscous flow around a ship advancing in shallow water. *Ocean Engineering*, 234, 109206. https://doi.org/10.1016/j.oceaneng.2021.109206

[37] Marelli, S., Lamas, C., Konakli, K., Mylonas, C., Wiederkehr, P., Sudret, B., 2024. UQLab user manual – Sensitivity analysis, Report UQLab-V2.1-106, Chair of Risk, Safety and Uncertainty Quantification, *ETH Zurich*, Switzerland.

[38] Parekh, J., Verstappen, R.W.C.P, 2023. Uncertainty quantification analysis for simulation of wakes in wind-farm using a stochastic RANS solver, compared with a deep learning approach. *Computers & Fluids*, 257, 105867. https://doi.org/10.1016/j.compfluid.2023.105867

[39] Katsuno, E.T., Lidtke, A.K., Duz, B., Rijipkema, D., Dantas, J.L.D., Vaz, G., 2021. Estimating parameter and discretization uncertainties using a laminar-turbulent transition model. *Computers & Fluids*, 230, 105129. https://doi.org/10.1016/j.compfluid.2021.105129

[40] Yang, M., Guo, M., Zhang, Y., Tian, Y., Yi, M., Le, J., Zhang, H., 2024. Uncertainty quantification and identification of SST turbulence model parameters based on Bayesian optimization algorithm in supersonic flow. *International Journal for Numerical Methods in Fluids*, 96(3), 277-296. https://doi.org/10.1002/fld.5245

[41] Romani, S., Morgut, M., Parussini, L., 2023. Uncertainty Quantification of Turbulence Model Applied to a Cavitating Hydrofoil. *IOP Conference Series: Materials Science and Engineering*, 1288, 012037. https://doi.org/10.1088/1757-899X/1288/1/012037